5th International Conference
on
Wind Turbine Noise
Denver 28 – 30 August 2013

Hybrid Methods for Noise Prediction in Aeroacoustic Simulations of Small Vertical Axis Wind Turbines

Johannes Weber. Institute of Process Machinery and Systems Engineering, Cauerstraße 4, 91058 Erlangen , Germany.
wb@ipat.uni-erlangen.de
Stefan Becker. Institute of Process Machinery and Systems Engineering, Cauerstraße 4, 91058 Erlangen, Germany.
sb@ipat.uni-erlangen.de
Christoph Scheit. Institute of Process Machinery and Systems Engineering, Cauerstraße 4, 91058 Erlangen, Germany.
sh@ipat.uni-erlangen.de
Jens Grabinger. Chair of Sensor Technology, Paul-Gordan-Straße 3/5, 91052 Erlangen, Germany.
jens.grabinger@fau.de
Manfred Kaltenbacher. Institute of Mechanics and Mechatronics, Wiedner Hauptstraße 8, 1040 Vienna, Austria.
manfred.kaltenbacher@tuwien.ac.at

Summary

Numerical methods are gaining more importance in the analysis of flow induced noise due to the increase in available computational power. The present work deals with two different numerical schemes of noise prediction of small vertical axis wind turbines using hybrid methods. As usual for hybrid aeroacoustic approaches, the flow field and acoustic calculations are carried out in separate software packages. For both schemes the time-dependent turbulent flow field is solved with Scale-Adaptive Simulation. The two schemes then differ in how the location of the acoustic sources and their propagation is calculated.
In the first scheme the acoustic source terms are computed according to Lighthill's acoustic analogy which gives source terms located on the original CFD grid. These source terms are projected onto a coarser acoustic grid on which the propagation is calculated by solving the wave equation.
In the second scheme the Ffowcs Williams-Hawking (FW-H) method is used which is based on a free field Green's function. The scheme uses a porous integration surface and implements an advanced time formulation. The far field acoustic radiation is calculated by extrapolation of the acoustic waves.
Both methodologies are compared with each other.

1. Introduction

In Germany wind energy will become more and more important due to the increasing awareness of the need for environmentally sustainable power generation, especially in light of the government's decision to phase out all nuclear power plants by 2022 following the Fukushima nuclear accident in 2011. In 2012, 31 GW [1] wind power was installed in Germany and shall be increased to 48 GW onshore and 13 GW offshore by 2022 [2]. This will lead to the installation of more wind turbines in vicinity of urban areas.
Therefore, it is important to improve the performance with respect to noise in order to prevent noise pollution of residential areas. Beside the conventional large wind turbines, small wind turbines are considered as a prominent solution for using wind energy at small scales in urban areas. Exploring this area of application, investigations so far have focused on vertical axis wind turbines (VAWT), which in comparison to horizontal axis wind turbines are characterized by the following advantages [3]:

- Insensitivity to the wind direction, which avoids the need of a yaw system
- Applicability in presence of turbulent streams
- Manufacture of VAWTs is cheaper [4]

In the recent years, experimental and numerical investigations were realized in the field of VAWTs by e.g. Simão Ferreira, who placed the focus on the research of dynamic stall [5]. Mertens investigated the performance of an H-Darrieus in the skewed flow on a roof [6]. Marnett studied a multiobjective numerical design of vertical axis wind turbine components in his PhD thesis [7].

In order to analyze the flow field and the radiated acoustic field of a vertical axis wind turbine, numerical simulations were performed in this work. Therefore, a transient flow simulation was carried out by application of the commercial computational fluid dynamics (CFD) software ANSYS-CFX [8]. Following that, two different in-house codes were used for acoustic post-processing. The first code is the finite-element multiphysics solver CFS++ [9, 22], which is based on Lighthill's analogy and has been developed at the Chair of Sensor Technology, University of Erlangen-Nuremberg. The second one is called SPySI (sound prediction by surface integration), which is predicated on the porous Ffowcs Williams-Hawking method. This scheme was established by Scheit [10, 11] and extended by Heinemann [12] at the Institute of Process Machinery and Systems Engineering, University of Erlangen-Nuremberg.
Such tools for noise prediction can be very useful in wind turbine design in order to optimize the system with respect to noise and aerodynamic performance.

2. Computational methods

In computational aeroacoustics (CAA) one can broadly distinguish two kinds of numerical methods: direct methods and hybrid methods. In the case of the direct approach, the compressible Navier-Stokes Equations, which completely describe all motions in a fluid as well as the flow generated acoustic field, are solved directly. The

drawback of this method consists in the need of resolving the whole range of length scales, which differ very strongly between the acoustic variables and the flow variables. Fluid mechanics is basically a near-field problem with small length scales compared to acoustics, which in general is a far-field problem. Due to the large disparity of scales, the direct approach requires very high computational power and therefore the application is limited to academic research and only for low Reynolds numbers [13].
In comparison, the hybrid methods – as used in this work - consist of two simulation steps. Firstly, the turbulent flow field is simulated and aeroacoustic sources are computed. Secondly, radiation of acoustic waves is calculated [14].

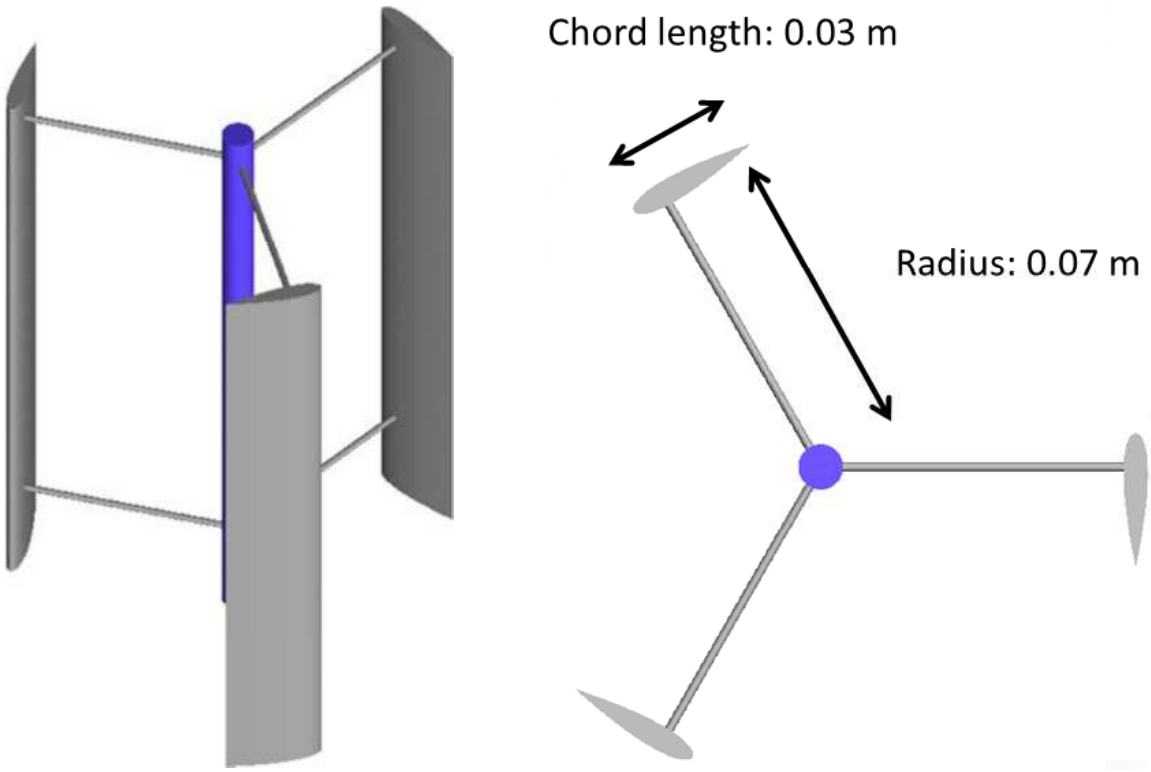

Fig. 1: Isometric (left) and top view (right) of H-Darrieus CAD geometry

2.1 Aerodynamic simulation

As a test case of the applicability of SPySI and CFS++ for vertical axis wind turbines, the design of an H-Darrieus wind turbine is used as illustrated in fig. (1) in order to compute the turbulent flow field with the finite-volume method solver ANSYS-CFX 14.0. The wind turbine consists of three symmetric NACA0018 airfoils, which are uniformly distributed in circumference. Figure (2) shows the circumferential computational fluid domain composed of a rotating and a stationary region, which are connected by a transient rotor stator interface. The inlet of the fluid domain is located on the left half of the outer circle and the inlet boundary condition was given by 5 m/s wind speed. At the outlet, an opening boundary condition was defined at relative pressure 0 Pa in order to allow backflow. The rotational speed of the airfoils was set to 1364 rpm. The tip-speed ratio is defined by $\lambda = \frac{2\pi n r}{v}$ which gives a value of 2.

A hexahedral mesh was generated by ANSYS ICEM and consisted of 809000 nodes. In order to ensure that the boundary layers at the blades and at the shaft are adequately resolved, the mesh is strongly refined to obtain a normalized wall distance $y^+ < 1$.

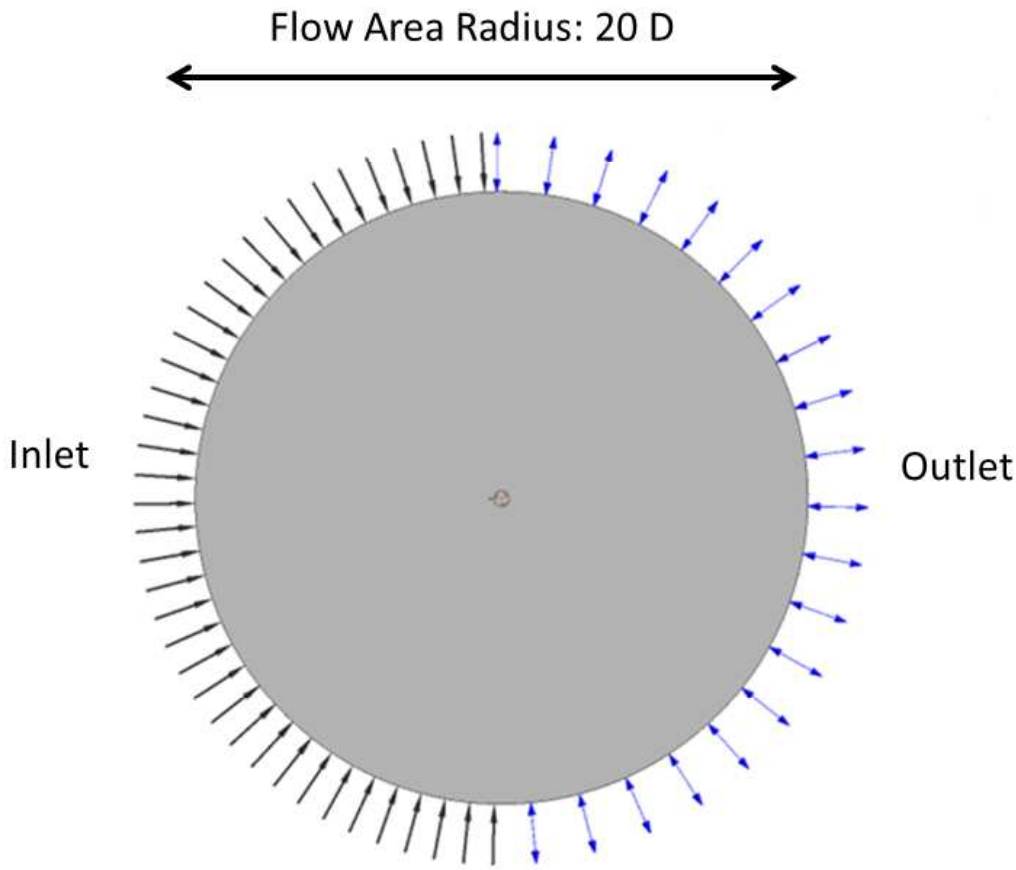

Fig.2: Computational domain of CFD-simulation

As the aeroacoustic solver CFS++ uses the simplified Lighthill stress tensor T_{ij} (see eq. 3) which assumes a constant density, a solution of the incompressible Navier-Stokes-Equation (NSE) is required. Contrary, SPySI needs a compressible solution.

Both simulations are solved with Scale Adaptive Simulation (SAS) established by Menter and Egorov [15, 16]. The SAS models are extended unsteady RANS models which differ in the resolved scales of turbulence. URANS methods only resolve unsteady, mean flow structures, which include coarse vortices. In contrast, SAS resolves dissipation of turbulent kinetic energy to smaller scales and eddies better. As spatial discretization scheme the bounded central difference scheme is used. The time step of $\Delta t = 1e^{-5}\ s$ was chosen, which corresponds to $CFL \sim 1$ [17] and to an angle increment of 0.08 degrees. As initial conditions the result of a previous RANS simulation was used. In order to assure a converged solution, flow quantities were monitored. Stable conditions were found after eight complete revolutions. The total time of both simulations was 1.7 s. After ensuring that the flow field was fully developed, the last 30000 time steps were calculated for the acoustic simulation. At every tenth of these flow field data was exported, which leads to 3000 time steps of $1e^{-4}\ s$ for the acoustic simulations.

2.2 Aeroacoustic formulation

The age of modern aeroacoustics is considered to begin with the seminal work of Lighthill in 1952 [18] and 1954 [19] on aerodynamically sound generated by jet engines. In his two-part paper he derived the concept of the acoustic analogy, which states that the noise produced by a turbulent flow field is equal to the noise generated by a distribution of quadrupole sources which can be calculated from the instantaneous fluctuations of the velocity field in the flow. Subsequently, Curle (1955) extended Lighthill's theory to take into account the influence of solid bodies [20]. In many technical applications such as helicopter rotors, aeroplane propellers, fans and turbines, moving solid surfaces are directly involved in the generation of noise. This is considered by the extension of Ffowcs Williams and Hawking (1969) [21].

In order to calculate the sound pressure spectra radiated by the H-Darrieus, the two acoustic analogies established by Lighthill on one hand and Ffowcs Williams and Hawkings on the other hand are used and will be presented in the following.

The computation of flow-induced noise according to Lighhill's analogy starts with his famous inhomogeneous wave equation for the sound pressure p'

$$\frac{1}{c_0^2}\frac{\partial^2 p'}{\partial t^2} - \frac{\partial p'}{\partial x_i^2} = \frac{\partial^2 T_{ij}}{\partial x_i \partial x_j} \tag{1}$$

The left hand side is equivalent to the homogenous wave equation. The right hand side which is the Lighthill tensor T_{ij} is the source term of the complete inhomogeneous wave equation. It was derived by Lighthill directly from the conservation of mass and momentum.

$$T_{ij} = P_{ij} + \rho u_i u_j - c_0^2 \delta_{ij} \rho' = \rho u_i u_j + (p' - c_0^2 \rho')\delta_{ij} - \tau_{ij}, \tag{2}$$

which consists of non-linear convective forces $\rho u_i u_j$, deviations in the speed of sound c_0, $(p' - c_0^2 \rho')$, viscous forces τ_{ij}, and the Kronecker delta δ_{ij}.

A further simplification of the Lighthill tensor can be accomplished in case of an isentropic flow at low Mach numbers. In this case, viscous effects $\tau_{ij}$are negligible and the term $(p' - c_0^2 \rho')$ is only relevant for anisotropic media and can be considered to be very small in air. Only the non-linear convective effects $\rho u_i u_j$ remain as sound sources and one obtains

$$T_{ij} \approx \rho_0 u_i u_j \tag{3}$$

To obtain a spatial discretization suitable for finite element-methods, a weak formulation of Lighthill's inhomogeneous wave equation is arranged. For this purpose, eq. (1) is multiplied by an appropriate element shape function w, integrated over the computational domain Ω and Stokes' integral theorem is applied [22].

$$\int_\Omega \frac{1}{c_0^2}\frac{\partial^2 p'}{\delta t^2} \mathrm{w} \mathrm{d}\Omega + \int_\Omega \frac{\partial w}{\partial x_i}\frac{\partial p'}{\partial x_i} \mathrm{d}\Omega - \int_\Gamma \frac{\partial p'}{\partial n} w \, \mathrm{d}\Gamma = -\int_\Omega \frac{\partial w}{\partial x_i}\frac{\partial T_{ij}}{\partial x_j} \mathrm{d}\Omega \tag{4}$$

In fig. (3) the computational domain Ω is depicted on which Lighthill's equation is solved using the finite element-method.

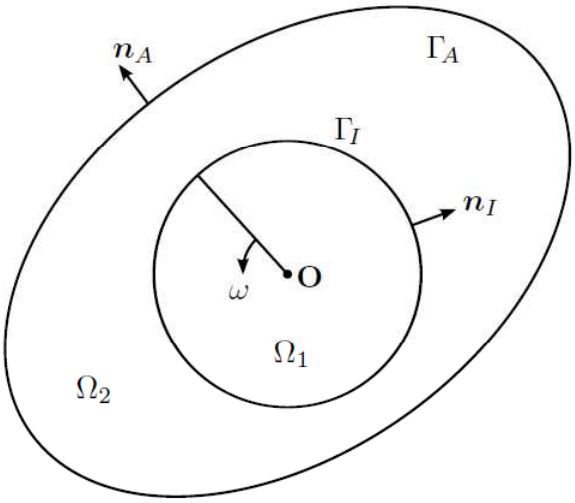

Fig.3: Schematic drawing of the computational domain Ω

For this purpose, the computational domain is divided into a rotating domain Ω_1 with the interface boundary Γ_I and a stationary domain Ω_2 with the outer boundary Γ_A. The rotation of Ω_1 is defined by the operator $r_t: \Omega_1 \rightarrow \Omega_1$, which characterizes the rotation at time by an angle $\theta = \omega t$, where ω denotes the angular speed of the rotating subdomain Ω_1. The reverse mapping is accomplished by the inverse operator r_{-t}, so that the rotating area can be written as a function of time

$$\Omega_1(t) = r_t \Omega_1(0) \tag{5}$$

A stationary frame of reference is used inside of Ω_2. As a result of the domain decomposition, both subdomains Ω_1, Ω_2 are discretized on their own. For this reason two disjoint domains with two solution functions p_1, p_2 are obtained.
The interface conditions applied at Γ_I are accomplished by the so-called mortar element method [23, 24], so that an exchange of sound waves between the grids of both domains (which are in general non-conforming on Γ_I) is ensured. The additional condition

$$\int_{\Gamma_I} \left(\frac{\partial p_1(r_{-t}x, t)}{\partial t} - \frac{\partial p_2(x, t)}{\partial t}\right) \mu d\Gamma = 0 \tag{6}$$

guarantees continuity in the trace of both solution functions p_1, p_2at the interface Γ_I with μ being a suitable test function. By introducing the Lagrange multiplier λ defined by

$$\frac{\partial \lambda}{\partial t} = \frac{\partial^2 p_1(r_{-t}x, t)}{\partial t \partial n_I} = \frac{\partial^2 p_2(x, t)}{\partial t \partial n_I}, \tag{7}$$

continuity in the flux of p_1, p_2 is achieved. In eq. (7), n_I denotes the outward normal unit vector on Γ_I. After that, the Lagrange multiplier λ is inserted into the third term of eq. (4) to arrive at the weak formulation.
In order to calculate the sound pressure spectra radiated by a vertical axis wind turbine, the numerical method based on FW-H acoustic analogy is presented in the following.

The porous Ffowcs Williams-Hawkings method is based on an integral solution of eq. (1). In comparison to the formulation of Lighthills equation not only the transient flow velocity, but also the pressure and density data is needed. Furthermore, a surface integral S wrapped around the source region V, which is defined by the scalar function $f(x_i, t)$ (see fig. 4),

$$\begin{aligned} f(x_i,t) &< 0 \quad \text{if } x_i \text{ is placed inside of the source region } V \\ f(x_i,t) &> 0 \quad \text{if } x_i \text{ is placed outside of the source region } V \\ f(x_i,t) &= 0 \quad \text{if } x_i \text{ is placed on the source region } S \end{aligned} \tag{8}$$

has to be chosen. The Heaviside function $H(f)$, $H(f) = 1 \; for \; f > 0$, $H(f) = 0 \; for \; f < 0$, ensures that no boundary conditions have to be fulfilled on the boundaries.

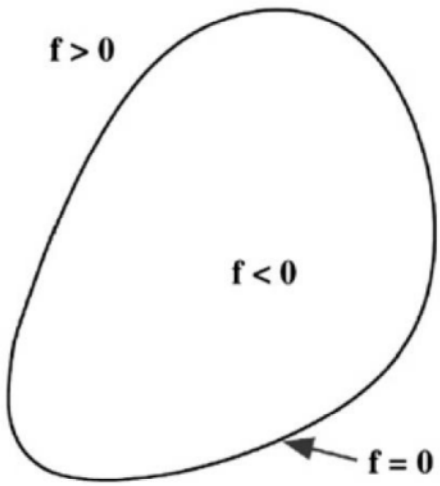

Fig.4: Boundary of a solid body inside the flow domain described by scalar function f

If one multiplies the Heaviside function $H(f)$ with the basic equations in the derivation of Lighthill's analogy, one obtains

$$\begin{aligned} \frac{\partial^2\{(\rho')H(f)\}}{\partial t^2} - c_0^2 \frac{\partial^2}{\partial x_i x_j}\{(\rho')\delta_{ij}H(f)\} \\ = \frac{\partial^2}{\partial x_i x_j}\{T_{ij}H(f)\} + \frac{\partial}{\partial t}\left\{\left(\rho\left(u_i - v_i^S\right) + \rho_0 v_i^S\right)\delta(f)\frac{\partial f}{\partial x_i}\right\} \\ - \frac{\partial}{\partial x_i}\left\{\left(P_{ij} + \rho u_j\left(u_i - v_i^S\right)\right)\delta(f)\frac{\partial f}{\partial x_i}\right\} \end{aligned} \tag{9}$$

Equation (9) is known as the differential form of Ffowcs Williams-Hawking, which expresses a generalized form of the Lighthill equation. Here, P_{ij} represents the

compressible stress tensor, u_i corresponds to the flow velocity, v_i^S symbolizes the integration surface velocity and $\delta(f)$is the Dirac function, which is the derivative of the Heaviside function. For calculation of radiation into free field eq. (9) can be solved with the free-space Green's function [25],

$$G(x,t) = \frac{\delta(t - |x_i - y_i| - \tau/c_0)}{4\pi|x_i - y_i|}, \tag{10}$$

where c_0 represents the ambient speed of sound and τ is the retarded time. Inside SPySi, Farassat's Formulation 1 [26] is implemented. For a stationary, porous integration surface S, the solution can be written as

$$p'(x_i,t) = p'_Q(x_i,t) + p'_L(x_i,t) + p'_T(x_i,t) \tag{11}$$

Here p'_T denotes the thickness noise and represents the physical mechanism of displacement of the fluid in the flow field by solid surfaces such as turbine blades. The term loading noise p'_L describes the physical mechanism of the force that acts on the fluid as a result of the presence of the surfaces of the body. The quadrupole distribution is denoted as p'_Q.
If volume forces are neglected and an integration over the surface S is performed, solutions for the thickness noise and loading noise are obtained:

$$4\pi p'_T(x_i,t) = \frac{\partial}{\partial t}\int_S \left[\frac{\rho_0 U_n}{r}\right]_{ret} dS \tag{12}$$

$$4\pi p'_L(x_i,t) = \frac{1}{c_0}\frac{\partial}{\partial t}\int_S \left[\frac{L_r}{r}\right]_{ret} dS + \int_S \left[\frac{L_r}{r^2}\right]_{ret} dS \tag{13}$$

The distance between the surface source and the observer position is represented by r and subscript n defines scalar contraction with the integration surface normal vector n_i. The variables U_i and L_i are introduced by Di Francescantonio [27] as following:

$$U_i = \frac{\rho}{\rho_0}u_i; \qquad L_i = P_{ij}n_j + \rho u_i u_n \tag{14}$$

To evaluate the acoustic signal run time between source and observer, there are two possible algorithms: the retarded time approach and the advanced time approach. In case of the advanced time algorithm

$$t_{adv} = t + \frac{r(t)}{c_0} \tag{15}$$

only one time step of CFD simulation data per acoustic evaluation is needed. Contrary, the retarded time algorithm requires several time steps at different source positions and therefore multiple time steps have to be in storage. SPySI uses the advanced time algorithm.

3. Results and discussion

To illustrate the transient flow field obtained by the CFD simulation, the evolution of the flow is presented in fig. 5. The left series shows the temporal evolution of the velocity in stationary frame, the right series depicts the pressure (the wind arriving from the left side in the pictures). As one can clearly see, there is strong vortex formation in the wake of the Darrieus turbine. Due to the conversion of kinetic energy to mechanic energy by the turbine, the mean flow velocity is reduced in an expanded downstream region. Furthermore, one can identify vortex shedding at the trailing edge of airfoils moving contrary to the wind (upper airfoils). At the airfoil in the upwind region (airfoil bottom left, 0 degree), a dynamic stall on the inner surface is seen. This stall induces formation of a vortex, which separates in the further temporal development, where the airfoil moves parallel to the mean flow. Afterwards, the stall at the inner surface arises directly again (airfoil bottom right, 0 degree), persists and expands for a whole revolution until it separates again. A pressure stagnation point remains at the leading edge at all times, except while separation of the stall vortex.

On the left side of fig. 6, the temporal evolution of the acoustic source terms, which are computed on the original CFD grid, is depicted. On the right side, the acoustic pressure calculated by CFS++ is illustrated. These images show the influence of the previously described flow phenomena on the acoustics.
The mentioned pressure stagnation point at the leading edges induces a sound source which is called leading edge interaction noise [28]. The second source region to mention is the trailing edge at the airfoils moving upstream, where the vortex shedding appears. Though these vortices are mostly dissipated by the time subsequent blades arrive collide with them, a weak interaction can be noticed. The vortex of the stall region at the inner side of the blades represents a further important sound source. When the angle of attack increases to almost 180 degrees, the vortex separates and a sound source region can be seen shedding from the blade [29]. Analogous observations can be made in the acoustic pressure images.

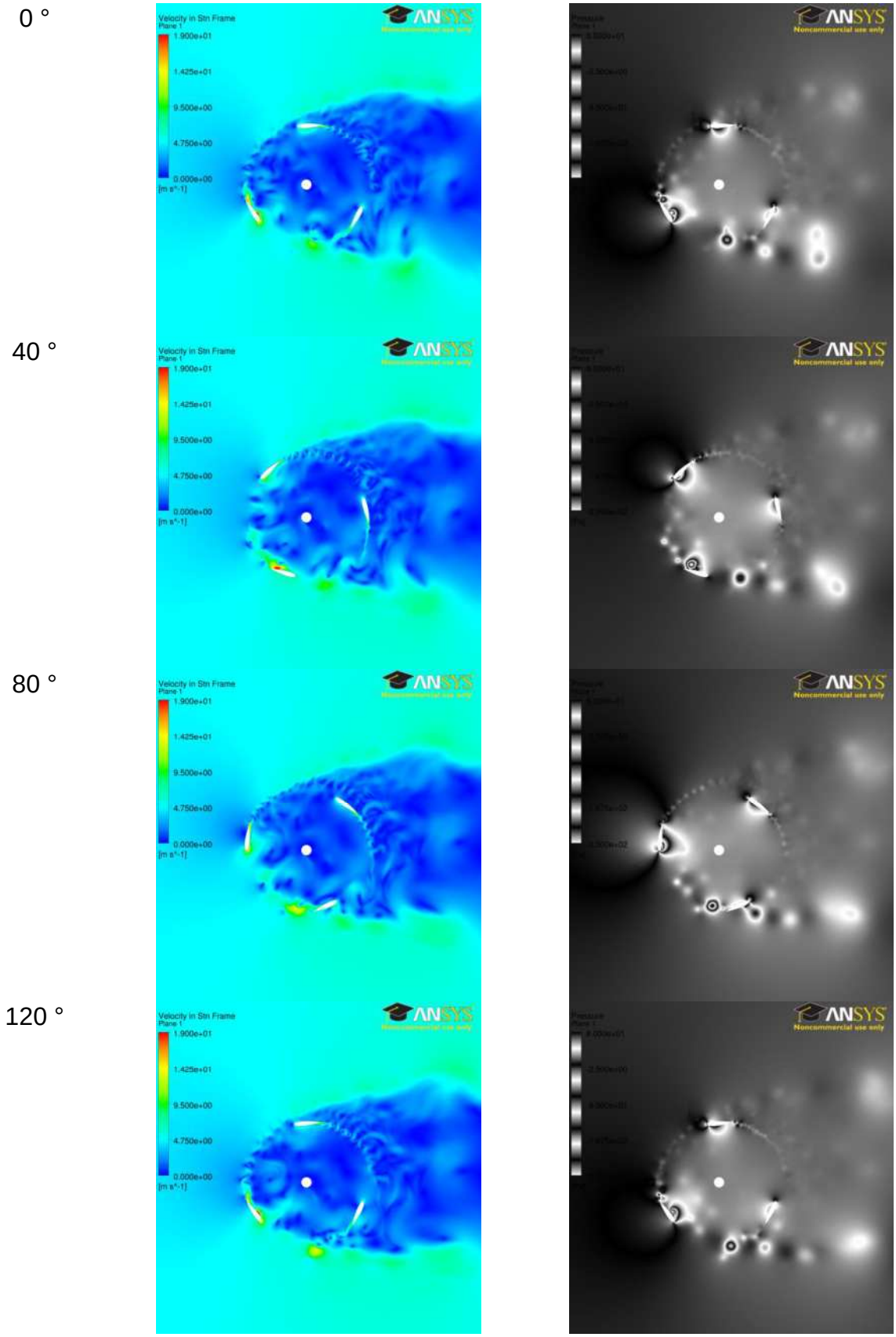

Fig 5.: Temporal development of the velocity in stationary frame (left) and pressure (right) in the rotating domain

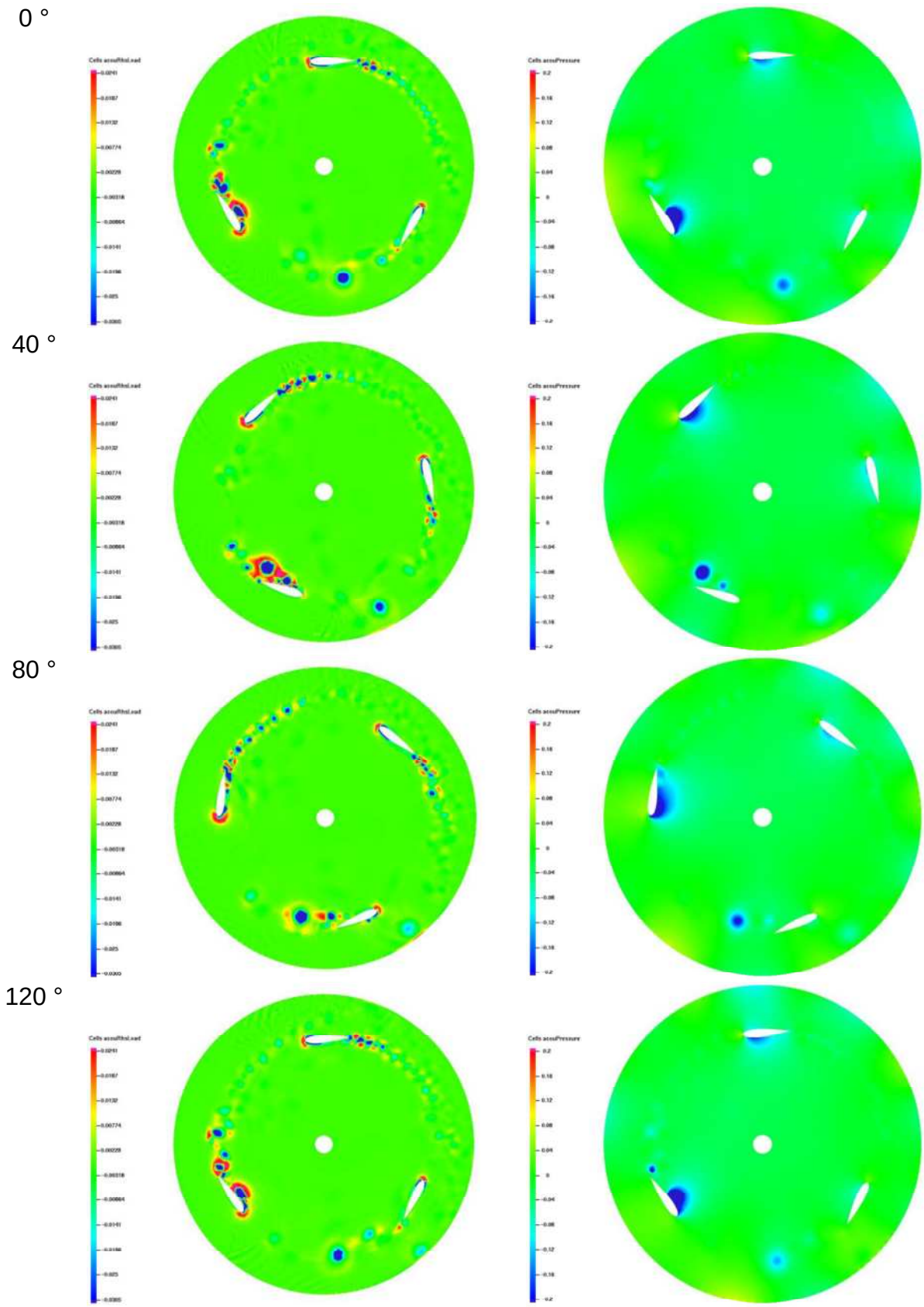

Fig. 6: Temporal development of the acoustic source terms (left) and acoustic pressure (right) in the rotating domain

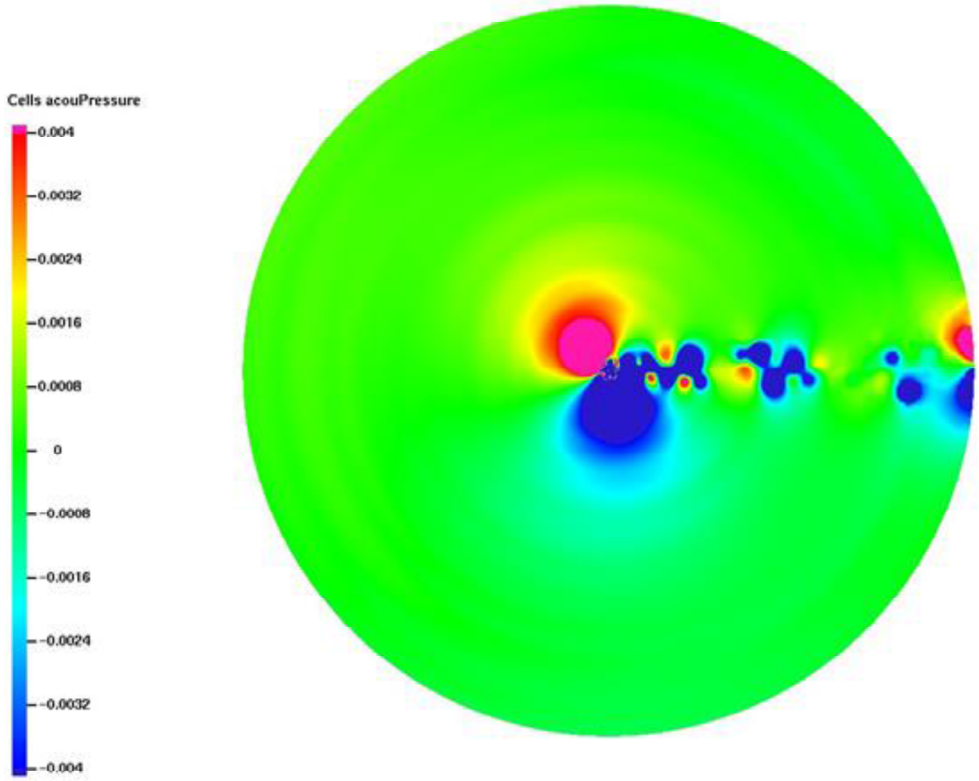

Fig. 7: Acoustic pressure in the whole computational domain

In figure 7 the acoustic pressure for the whole domain is illustrated. The sound pressure is radiated as a dipole source. Behind the wind turbine, acoustic pressure variations corresponding to the Karman-vortex street occur.

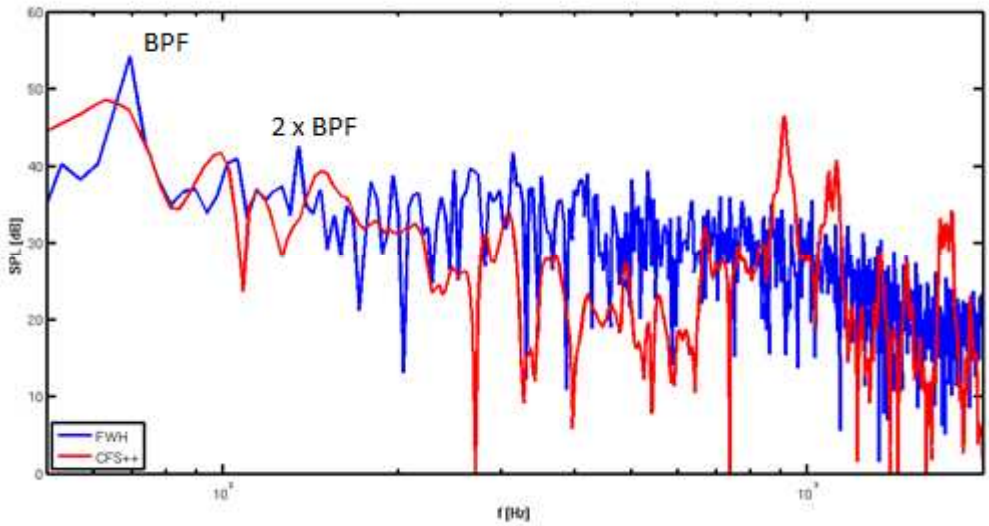

Fig. 8: Sound pressure level spectra of FWH and CFS++

In order to compare both methodologies qualitatively, the sound pressure level spectrum obtained from simulations of FWH and CFS++ is depicted in fig. 8. In general, there is a good agreement between both simulations. The first tonal peak relates to the blade passage frequency of 68.2 Hz and the second peak to the second harmonic of the blade passage frequency.

4. Conclusions

Numerical investigations of sound generation of an H-Darrieus wind turbine have been performed in order to get a better physically understanding. To this end, acoustic analogies of Lighthill and Ffowcs Williams and Hawking have been applied to CFD simulation data. In summary, there is a good agreement between both acoustic approaches. Separation-stall noise, vortex shedding noise at the trailing edge as well as leading edge noise were identified as main source regions of the H-Darrieus. Future investigations will focus on the impact of each of these sources on the overall noise emission. Using these CFD and CAA tools aerodynamic and aeroacoustic optimization can be accomplished with regard to the design of vertical axis wind turbines.

References

[1] The European Wind Energy Association (2013) *Wind in power – 2012 European statistics*

[2] German Federal Network Agency (2012) *Administrative decision of the scenario outlook in English*

[3] Paraschivoiu, I. (2002) *Wind Turbine design – With Emphasis on Darrieus Concept* Presses Internationales Polytechnique

[4] Milborrow, D. (1995) *Vertical axis wind turbines* WindStats Newsletter 8, pp. 5-8

[5] Ferreira, C.J. (2009) *The near wake of the VAWT -2D and 3D views of the VAWT aerodynamics* PhD thesis, TU Delft

[6] Mertens, S. (2006) *Wind Energy in the Built Environment* PhD thesis, TU Delft

[7] Marnett, M. (2012) *Multiobjective Numerical Design of Vertical Axis Wind Turbine Components* PhD thesis, RWTH Aachen

[8] ANSYS, ANSYS, fourteenth ed. <www.ansys.com>

[9] Escobar, M. (2007) *Finite Element Simulation of Flow-Induced Noise using Lighthill's Acoustic Analogy* PhD thesis, University of Erlangen-Nuremberg

[10] Scheit, C. (2007) *Implementation of a Ffowcs Williams and Hawkings (FW-H) method for aeroacoustic prediction.* Master of Science thesis, University of Erlangen-Nuremberg

[11] Scheit, C., Karic, B. and Becker, S. (2011) *Effect of blade wrap angle on efficiency and noise of small radial fan impellers – A computational and experimental study* Journal of Sound and Vibration, No. 331, No. 5, pp. 996-1010

[12] Heinemann, T. (2011) *Implementation of a Ffowcs Williams and Hawkings (FW-H) formulation for moving surfaces.* Diploma thesis, University of Erlangen-Nuremberg

[13] Tam, C. (2004) *Computational Aeroacoustics: An overview of computational challenges and applications.* International Journal of Computational Fluid Dynamics, Vol. 18, No. 6, pp. 547-567

[14] Wagner, C., Hüttl, T., Sagaut, P. (2007) *Large-Eddy Simulation for Acoustics,* Cambridge University Press

[15] Menter, F. and Egorov, Y. (2010) *The Scale-Adaptive Simulation Method for Unsteady Turbulent Flow Predictions. Part 1: Theory and Model Description* Flow Turbulence and Combustion, Vol. 85, No. 1, pp. 113-138

[16] Menter, F. et al. (2010) *The Scale-Adaptive Simulation Method for Unsteady Turbulent Flow Predictions. Part 2: Application to Complex Flows* Flow, Turbulence and Combustion, Vol. 85, No. 1, pp. 139-165

[17] Courant, R., Friedrichs, K. and Lewy, H. *Über die partiellen Differentialgleichungen der mathematischen Physik* Mathematischen Annalen, Vol. 100, No. 1, pp 32 – 74
[18] Lighthill, J. M. (1952) *On Sound Generated Aerodynamically I. General Theory* Proceedings of the Royal Society, Vol. 211, No. 1107, pp. 564–587.
[19] Lighthill, J. M. (1954) *On Sound Generated Aerodynamically II. Turbulence as a Source of Sound* Proceedings of the Royal Society, pp. 1–32.
[20] Curle, N. (1955) *The Influence of Solid Boundaries upon Aerodynamic Sound* Proceedings of the Royal Society, Vol. 231, No. A, pp. 505–514.
[21] Ffowcs Williams, J. E. and Hawkings, D. L. (1969) *Sound Generation by Turbulence and Surfaces in Arbitrary Motion* Philosophical Transactions of the Royal Society, Vol. 264, No. 1151, pp. 321–342.
[22] M. Kaltenbacher, M. Escobar, I. Ali and S. Becker (2010), *Numerical Simulation of Flow-Induced Noise Using LES/SAS and Lighthill's Acoustics Analogy*, International Journal for Numerical Methods in Fluids, Vol. 63(9), pp. 1103–1122
[23] Flemisch, B., Kaltenbacher, M., and Wohlmuth, B. I (2006) *Elasto-acoustic and acoustic-acoustic coupling on nonmatching grids,* Int. J. Numerical Methods in Engineering, Vol. 67, No. 13, pp. 1791–1810.
[24] Triebenbacher S., et al. (2010) *Applications of the Mortar Finite Element Method in Vibroacoustics and Flow Induced Noise Comptations,* Acta Acustica united with Acustica2010. Vol.96, pp.536-553.
[25] Ehrenfried, K. (2004) *Strömungsakustik (Aeroacoustics*) Mensch & Buch Verlag, pp. 145-159
[26] Farassat, F. (1996) *Introduction to generalized functions with applications in aerodynamics and aeroacoustics,* Technical Report, NASA
[27] Di Francescantonio, P. (1997) *A New Boundary Integral Formulation for the Prediction of Sound Radiation,* Journal Sound and Vibration, Vol.202, No. 4, pp. 491 – 509.
[28] Blake, W.K. (1986) *Mechanics of flow-induced sound and vibration, volume 2*. Academic Press, New York.
[29] Brooks, T.F., Pope, D.S., Marcolini, A. (1989) *Airfoil Self-Noise and Prediction,* NASA Reference Publication 1218